Flow boundary conditions for chain-end adsorbing polymer blends

Xin Zhou, Denis Andrienko,[a)] Luigi Delle Site, and Kurt Kremer

Max-Planck-Institut für Polymerforschung, Ackermannweg 10, 55128 Mainz, Germany

Using the phenol-terminated polycarbonate blend as an example, we demonstrate that the hydrodynamic boundary conditions for a flow of an adsorbing polymer melt are extremely sensitive to the structure of the epitaxial layer. Under shear, the adsorbed parts (chain ends) of the polymer melt move along the equipotential lines of the surface potential whereas the adsorbed additives serve as the surface defects. In response to the increase of the number of the adsorbed additives the surface layer becomes thinner and solidifies. This results in a gradual transition from the slip to the no-slip boundary condition for the melt flow, with a nonmonotonic dependence of the slip length on the surface concentration of the adsorbed ends. © *2005 American Institute of Physics.*
[DOI: 10.1063/1.2009735]

I. INTRODUCTION

The equations of continuum fluid mechanics are incomplete without appropriate boundary conditions. In most situations it is required that both normal and tangential components of the relative fluid velocity vanish at the surface.[1] This, so-called stick or no-slip boundary condition, has successfully accounted for most of the experimental facts. It is, however, empirical by nature: there are no theoretical arguments in favor of the no slip; moreover, it has been known since Maxwell's time[2] that even a simple kinetic theory of gases predicts the nonzero value of the tangential velocity at the wall.

Providing some of the insight into the question, kinetic theory fails already for simple fluids adjacent to a rigid solid. In a more general context, multiple scattering from the individual wall molecules remains the major problem of most analytical theories. In this situation computer-simulation techniques are able to advance our knowledge of the processes occurring at the surfaces.

Indeed, molecular dynamics (MD) simulations demonstrated that, in the case of simple fluids, the flow boundary conditions are sensitive to the fluid epitaxial order[3] as well as the wall structure.[4] The situation, however, becomes much more complicated for polymers at the surfaces, because of the much richer molecular arrangement (e.g., formation of brushes,[5] various adsorbed and depleted layers[6]) as well as much stronger correlation between the atoms right at the wall with the rest of the surface layer.[7–9]

Recent MD studies of the end-adsorbing polymer melts, performed with a novel quantum-based multiscale approach for the surface/polymer interaction, showed that at least two mechanisms contribute to the hydrodynamic boundary conditions.[10] The attached parts of the chains scatter on the surface potential while moving along its equipotential lines. This induces the density and the chain conformation modulation in the adsorbed layer, and energy is lost from these modulations through the coupling to the thermostat, similar to the situation observed for a generic model of adsorbed surface layers.[11] On the other hand, single-end-grafted chains of polymer brushes undergo a coil/stretch transition and disentangle from the melt at a given shear rate,[12–15] favoring the slip boundary condition. Though investigated for the special case of end-adsorbing polycarbonate on nickel, a similar scenario will occur for block copolymers with an adsorbing block.

Valid for *monodispersed* melts, this picture does not account for the usual melt polydispersity, persity, which is an outcome of all synthetic polymerization reactions. Moreover, in many situations the self-blending of polymer melts is used.[16] A small amount of a lower weight polymer improves the melt processability without significantly affecting its mechanical properties. It, however, alters the structure of the surface layer[17] modifying the hydrodynamic boundary conditions for the melt flow. These changes shall be taken into account at the later stages of melt processing.[18]

In this work we focus on the hydrodynamic boundary conditions for polymer *blends* adsorbed on a solid substrate. For this purpose we consider a particular system, that is, bisphenol-A polycarbonate (BPA-PC) melt sheared over a (111) nickel surface. Our choice of polycarbonate as a test system is twofold. First, it is widely used in various applications[19] and, therefore, has been intensively studied both experimentally[20] and theoretically.[21–25] In particular, the shear of monodispersed melts[10] and the structure of the static epitaxial layer for monodispersed melts[26,27] and blends[17] have already been considered. Second, although it is a specific system, it has a number of important generic features, which also apply to a realistic description of many polymer brushes composed of block copolymers.

Our prime goal is to relate the structure of the adsorbed layer, which changes in the presence of the low molecular weight additive, to the hydrodynamic boundary conditions for the melt flow, specified by the slip length and the surface friction coefficient.

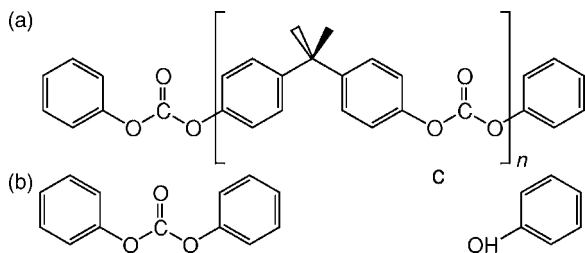a)Electronic mail: denis.andrienko@mpip-mainz.mpg.de

123, 104904-1

(a)

(b)

FIG. 1. Chemical structures: (a) phenol-terminated bisphenol-A polycarbonate (in this study $n=1, 5, 20$); (b) diphenyl carbonate (DPC); and (c) phenol.

TABLE I. Studied systems. $\sigma=4.41$ Å.

N_1, N_2	n_1, n_2	L_z, σ
20	400	80.91
20, 5	400, 76	85.15
20, 1	400, 239	84.97
20, DPC	400, 521	84.69
20, Phenol	400, 1186	83.79

II. SIMULATION DETAILS

We consider four types of polymer mixtures. The host polymer (major component) is the phenol-terminated BPA-PC of $N_1=20$ repeat units. The second (minor) component is one of the following: BPA-PC of $N_2=5$ repeat units, one repeat unit, diphenyl carbonate (DPC), or phenol, all shown in Fig. 1. For all mixtures, we use $n_1=400$ chains of the major component; the number of molecules of the minor component n_2 is then adjusted to provide (approximately) 5% of the total weight of the system. Exact numbers are given in Table I.

To simulate the melt, we use the previously developed coarse-graining model, in which each monomer is replaced by four beads that correspond to isopropylidene, carbonate, and the two linking phenylenes. Interaction potentials, bead sizes, and coarse-graining procedure are described in Refs. 26 and 27. The bead-wall interaction potentials are obtained from *ab initio* density-functional calculations. All *internal* beads experience strong increasing repulsion below 3.2 Å, either due to the nature of the molecular interaction or due to the steric hindrance by other beads. Only the chain ends are absorbed, on the wall. The wall-end interaction potential is expanded in a two-dimensional (2D) reciprocal lattice space of (111) nickel surface and has the following form:

$$U(x,y,z) = \sum_i U_i(z) f_i(x,y), \qquad (1)$$

where $i=0, 1, 2$ corresponds to the reciprocal vectors of different lengths; $f_0=1$, $f_1=\cos(\bar{x}-\bar{y})+\cos(\bar{x}+\bar{y})+\cos 2\bar{y}$, and $f_2=\cos(\bar{x}-3\bar{y})+\cos(\bar{x}+3\bar{y})+\cos 2\bar{x}$, where $(\bar{x},\bar{y})=(2\pi/a)\times(x,y/\sqrt{3})$,

$$U_0 = \begin{cases} 5/3\,\epsilon_r[2/5(z_0/z)^{10} - (z_0/z)^4 + 3/5] - \epsilon_0, & z<z_0 \\ \epsilon_0/2[\cos(\pi(z_c-z)/(z_c-z_0)) - 1], & z_0 \leq z < z_c \end{cases},$$

$$U_{1,2} = \begin{cases} -\epsilon_{1,2}, & z<z_0 \\ \epsilon_{1,2}/2[\cos(\pi(z_c-z/z_c-z_0)) - 1], & z_0 \leq z < z_c \end{cases}.$$

The interaction potential obtained using *ab initio* calculations is well reproduced by the following set of parameters: $\epsilon_r=1.5$ eV, $\epsilon_0=0.7$ eV, $\epsilon_1=-7/45$ eV, and $\epsilon_2=-2/45$ eV. For details, see Refs. 10, 24, and 28.

The melts are confined to a slit pore of thickness L_z with the walls perpendicular to the z axis. Periodic boundary conditions are employed in x and y directions. The x and y box dimensions are set to $L_x=22.23\sigma$ and $L_y=21.72\sigma$ with $\sigma=4.41$ Å, which corresponds to a (111) hexagonal lattice of nickel with 39 and 22 unit cells. The number density of

beads is $n=0.85$, which corresponds to 1.05 g/cc, the experimental density at the processing temperature, 570 K. The units are chosen such that $k_BT=1$ with $T=570$ K and σ is unity.[26,27]

Starting configurations are generated by randomly placing the chains in the simulation box. A short run is then used to remove the bead-bead overlaps.[27] The production run is performed in the *NVT* ensemble with Langevin thermostat with a friction of $0.5\tau^{-1}$, where τ is the unit of time in the simulations. The thermostat is switched off in the shear direction. The velocity-Verlet algorithm with the time step $\Delta t=0.005\tau$ is used to integrate the equations of motion. After equilibration for about $2\times10^5\tau$, the shear is applied by moving the top and bottom walls in opposite directions at a constant velocity v_w, so that the shear rate is $\dot{\gamma}=2v_w/L_z$. The wall velocity is the same as in our previous studies of *monodispersed* BPA-PC melts,[10] $v_w\tau/\sigma=0.01$. The corresponding shear rate can be obtained from the time mapping $1\tau\approx25$ ps (see Ref. 29 for details). Using this mapping we obtain $\gamma\approx10^7$ s^{-1}. Taking into account that the average chain length in a BPA-PC melt is $N\sim70$ and the corresponding chain reptation time $\tau_d\sim N^{3.4}$ is almost by two orders of magnitude larger than that of the $N=20$ chains. Equivalently, the shear rate would be reduced to 10^5 s^{-1}, close to the value used for industrial processing of BPA-PC, $\sim10^4$ s^{-1}. Note that smaller shear rates either have no significant effect on the adsorbed layer or are difficult to analyze, due to significant error bars for the velocity profiles.

III. RESULTS

A. Blends with different additives

We first have a look at the structure of the surface layer. Figure 2 shows a typical chain-end density profile for a monodispersed melt ($N=20$). The chain-end density has a sharp peak next to the wall, which is due to the strong adsorption of the ends; the region with no ends follows; finally, the bulk concentration is reached at a distance of the order of the radius of gyration, $R_g\approx6.2\sigma=27$ Å. The inset illustrates how this profile changes in the presence of the additives: the shorter the chains of the *minor* component, the more of them adsorb on the wall. This of course results in a decrease of the number of the adsorbed chain ends of the *major* component, in agreement with our earlier studies[17] except for the phenol additive, for which we previously observed a weak increase in the number of the adsorbed chain ends of the major component compared to the DPC case.[30] The representative snapshots of the systems with and without shears are shown in Fig. 3. Snapshots (a) and (c) illustrate the thinning of the
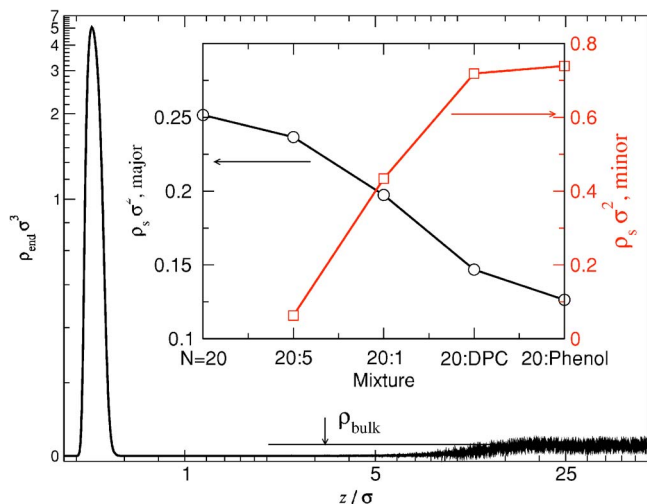
FIG. 2. Typical chain-end density profile ($N = 20$). The log scale is used to show the bulk density and the depleted region on the same plot. The inset depicts the change in the surface density (number of the adsorbed chain ends per unit area) for the minor and major components.

FIG. 4. Velocity profiles normalized to the wall velocity. The inverse of the surface friction coefficient $\beta^{-1} \sim 1 - v_s/v_w$ (circles) and the shear stress f_x/S (squares) are shown in the inset. To calculate the velocity profiles we average over all beads, independent of the nature of a particular bead.

adsorbed layer due to the decrease in the number of the adsorbed chain ends of the major component.[31] After shear is applied, the one-end-attached chains disentangle from the melt, stretch, and form a thin lubricating layer between the bulk and the chains adsorbed with two ends [see snapshots (b) and (d)]. Corresponding changes can also be detected by observing the center-of-mass profiles.[10]

Having resolved the structure of the adsorbed layer, we shall turn our attention to the velocity profiles, which are shown in Fig. 4. For all mixtures, the profiles have features similar to those of monodispersed systems.[10] Next to the wall the velocity is practically constant, since the adsorbed chains are dragged by the wall. Immediately after the plateau, the velocity profile becomes a linear function of z. The velocity of the beads at the wall, v_s, is smaller than the wall velocity v_w, i.e., the chain ends slide over the wall, moving between the hollow and bridge sites of the potential (the difference in the adsorption energies of these two sites is rather small, of the order of $2kT$; see the contour plot in Fig. 5). In case of

the monodispersed system and 20:5 mixture we have $v_s/v_w \sim 0.5$. This ratio increases for the 20:1 mixture and reaches 1 for the diphenyl carbonate and phenol additives.

We can write the stationary shear stress τ_{xz} (force per unit area) as[32]

$$\tau_{xz} \equiv f_x/S = \beta(v_w - v_s), \qquad (2)$$

where β is the friction coefficient between the adsorbed layer and the wall, and S is the surface area. Since the density of the minor component in the bulk is small (5% in weight and most of it is adsorbed on the walls) the bulk properties of the melt do not change significantly from mixture to mixture. Indeed, the shear stress τ_{xz} is practically independent of the molecular weight of the additive (see the inset to Fig. 4). Therefore, the change of v_s is due to the different values of the friction coefficient β, which increases significantly for short additives.
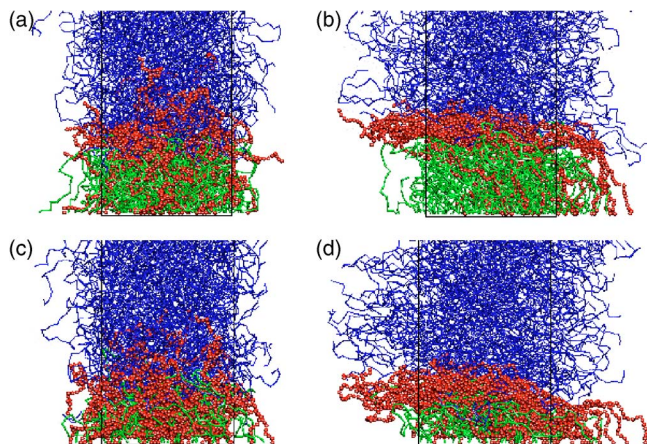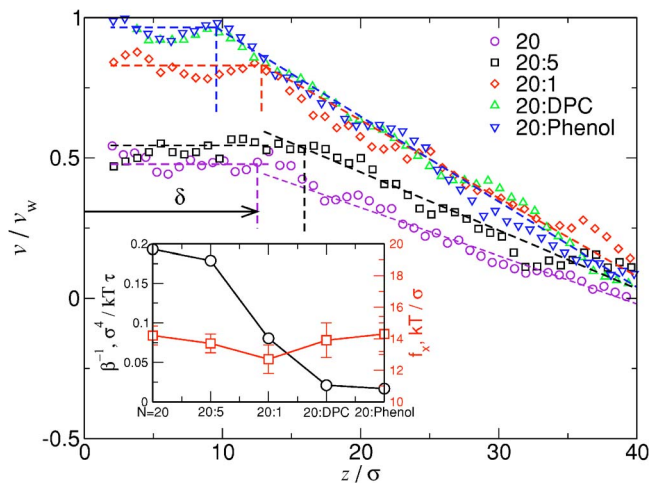

FIG. 3. Snapshots of the mixtures: 20:5 without (a) and with (b) shears, and 20:phenol without (c) and with (d) shears. Polymer chains are divided into three populations: chains which adsorb both ends (green), only one end (red), and no ends on the surface (blue).
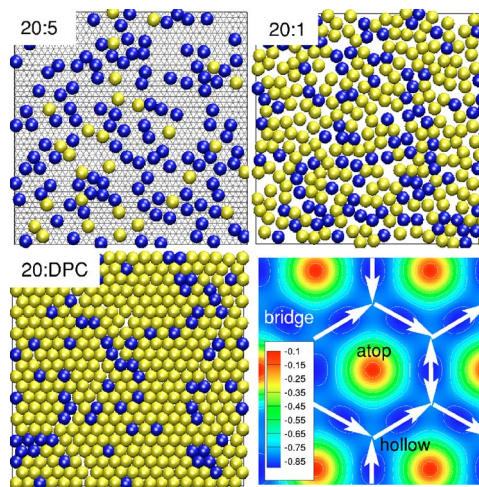

FIG. 5. Snapshots of the chain ends adsorbed on the walls. Blue beads: major component; yellow beads: minor component. The bead sizes correspond to their van der Waals radii. The triangular grid depicts the lattice of the (111) nickel surface. The contour plot illustrates the bead-wall potential used in simulation, together with the possible paths for the adsorbed beads. The contour levels are in electron volts, 1 eV $\approx$ 20 kT.

This increase is, in fact, rather unexpected: the adsorbed additives reduce the number of the attractive sites available for the major component and, in principle, shall screen the effective interaction of the melt with the surface. A weaker interaction should result in a smaller, compared to the mono-dispersed melt, friction coefficient. This, however, does not happen in practice: the systems with the phenol or diphenyl carbonate additives, which basically cover about 80% of the wall, have the biggest friction coefficient.

To understand why this happens, let us have a look at the structure of the beads adsorbed on the surface. Figure 5 shows the snapshots of the representative mixtures. The difference between the systems is now clear: the adsorbed layer of the 20:5 mixture has a structure similar to a two-dimensional (2D) gas; the packing of the 20:1 mixture is more dense, but still disordered, similar to a 2D liquid; and for the 20:DPC as well as 20:Phenol (not shown) mixtures the concentration of the adsorbed chain ends is so high that they form a 2D crystalline layer. The hexagonal lattice of this layer has the lattice constant of $2a$, where a is a lattice constant of the (111) nickel surface, which is of the order of the van de Waals diameter of the adsorbed beads, i.e., the close-packed surface layer is not frustrated energetically, or, in other words, the surface potential and the surface layer have commensurable lattices.

B. Different concentrations of the phenol additive

To quantify our results even further, we have also studied mixtures with different concentrations of the phenol additive. In these mixtures the surface densities of the adsorbed chain ends and phenol molecules are monotonic functions of the total number of phenol molecules in the system. Hence, they can be varied with a good precision, which helps to analyze the systems in a more systematic way.

The systems were prepared in a similar manner: the number of the phenol molecules was adjusted to provide different percentages of the total weight of the system, ranging from 1% to 20%. Because of the finite size of the simulation box and phenol adsorption, the concentration of the phenol molecules in the bulk is always smaller than the one used for the system preparation. We therefore used this number (from 1% to 20%) only to label a particular system. The important quantities are of course the surface density of the adsorbed chain ends and phenol molecules.

In addition to the velocity profiles we have calculated the two-dimensional radial distribution function of the adsorbed molecules,

$$g(r) = \frac{2}{n^2} \frac{L_x L_y}{S(r)} \left\langle \sum_{i=0}^{n-1} \sum_{j=i+1}^{n} p_{ij}(r) \right\rangle, \tag{3}$$

where $r_{ij} = \sqrt{(x_i - x_j)^2 + (y_i - y_j)^2}$, $S(r) = \pi[(r+\Delta r)^2 - \pi r^2]$ is the bin area, $\Delta r = r_{max}/N_{bins}$ is the bin width, and $p_{ij}(r) = 1$ if $r < r_{ij} < r + \Delta r$ and zero otherwise. The sum is performed over the adsorbed beads (chain ends and phenol molecules) only, i.e., $z_{i,j} - z_{wall} < \sigma$; n is the number of the adsorbed beads; and $\langle \cdots \rangle$ denotes the ensemble average.
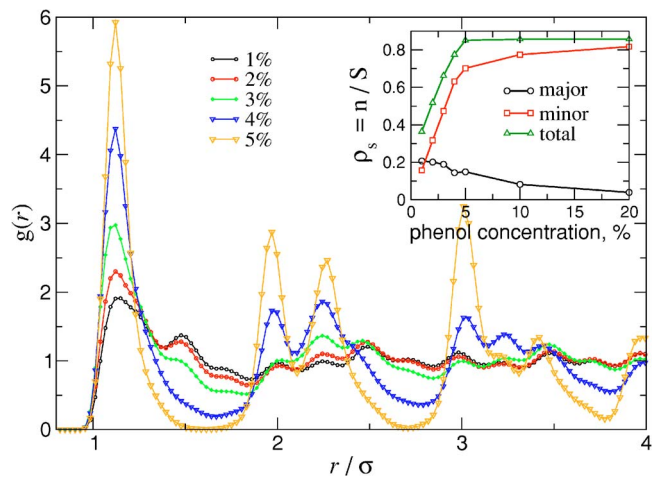

FIG. 6. Two-dimensional radial distribution function of the adsorbed chain ends. Inset shows the surface densities (number of adsorbed beads per unit area) of the adsorbed ends as a function of the phenol concentration.

To further characterize the quality of the hexagonal packing we have also calculated the orientational order parameter[33]

$$S_6 = \left\langle \frac{\left| \sum_{i=0}^{n-1} \sum_{j=i+1}^{n} q_{ij} \exp(i6\phi_{ij}) \right|}{\sum_{i=0}^{n} \sum_{j=i+1}^{n} q_{ij}} \right\rangle, \tag{4}$$

where ϕ_{ij} is the angle between the vector r_{ij} and a given axis in the xy plane, $q_{ij} = 1$ if r_{ij} belongs to the first peak of the radial distribution function (in our case between 0.5σ and 1.5σ), and zero otherwise. Note that $S_6 = 1$ in the case of a perfect hexagonal order whereas $S_6 = 0$ indicates the complete lack of such order.

The radial distribution functions are shown in Fig. 6. The increase of the total number of the adsorbed molecules results in a gradual solidification of the surface layer. The 4% system ($\rho_s = 0.775\sigma^{-2}$) has a two-dimensional solid layer formed at the surface, as it can be seen from the peaks at $2l$ and $\sqrt{3}l$, where l is the position of the first peak. Further increase of the amount of adsorbed molecules merely improves the hexagonal close packing and after the 5% system ($\rho_s = 0.851\sigma^{-2}$) the close packing of the surface is reached, i.e., the radial distribution function does not change anymore. The ratio between the number of the adsorbed chain ends and the adsorbed phenol molecules, however, still decreases, as it can be seen from the inset in Fig. 6. In case of the blends, the solidification of the surface layer occurs for the 20:DPC mixture.

The force on the wall and the velocity of the adsorbed layer are shown in Fig. 7, together with the orientational order parameter S_6. The orientational order parameter S_6 confirms that the solidification of the surface layer occurs for the 4% system, and the saturation for the 5% system, in agreement with the behavior of the radial distribution functions.

From the dependence of the relative velocity of the adsorbed layer on the surface density of the adsorbed
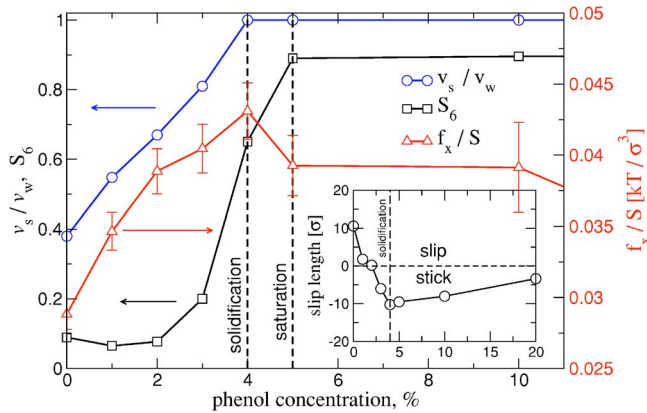
FIG. 7. Normalized (to the wall velocity) velocity of the adsorbed layer v_s/v_w (circles), orientational order parameter S_6 (squares), and the force per unit area on the wall (triangles). Inset: slip length, defined as a distance at which the melt velocity extrapolates to zero.

molecules one can see that once the epitaxial layer is in a solid state, it follows the wall, i.e., we have the stick boundary conditions for the surface layer. However, before the solidification, the velocity of the adsorbed layer is smaller than the wall velocity and is roughly proportional to the total concentration of the adsorbed chain ends.

Similar to the relative velocity, the friction force on the wall increases with the increase of the total amount of the adsorbed beads. However, it does not reach a constant value at the point of solidification of the surface layer, as the relative velocity does, but starts to decrease, with the decrease rate proportional to the ratio of the number of the adsorbed chain ends to the number of the adsorbed phenol molecules. This is due to the fact that the amount of the *long* chains adsorbed on the wall still decreases and the surface layer disentangles from the bulk of the melt.

Finally, we have also calculated the slip length, which is defined as the extrapolation length of the linear velocity profile in the bulk to zero and is often taken as a parameter in macroscopic descriptions of a fluid flow. The concentration dependence of the slip length is shown in the inset of Fig. 7. Two regimes can be clearly seen. First, at a low concentration of the adsorbed chain ends (e.g., in case of a pure melt, $N=20$) the melt slips over the wall. If we increase the surface concentration of the adsorbed beads, the slip length decreases and becomes zero at some concentration, i.e., we effectively have the no-slip boundary conditions for the melt flow. This point, however, does not coincide with the actual locking of the surface layer, which we observe only when it solidifies. The reason can be seen from the shape of the velocity profiles: let us denote the thickness of the adsorbed layer as δ and the velocity of this layer as v_s. Then the bulk velocity can be written as $v=v_s(L_z-2z)/(L_z-2\delta)$. The slip length b, obtained from the condition $v(z=-L_z/2-b)=v_w$, reads

$$b = (v_w/v_s - 1)L_z/2 - \delta v_w/v_s. \tag{5}$$

It can be seen that two mechanisms contribute to the total slip length b. The first one is due to the apparent slip of the

adsorbed layer over the surface. The second, negative, contribution is due to the finite thickness of the adsorbed polymer layer. As we add the additives, the adsorbed layer shrinks, giving rise to a higher slip; the relative velocity of the adsorbed layer, however, drops down much faster. Combined, these two mechanisms result in a zero slip for some intermediate concentration of the adsorbed chain ends and a negative slip for higher surface concentrations.

After the solidification, the adsorbed layer follows the wall, i.e., $v_w=v_s$. However, if we further increase the amount of the phenol additive, the ratio between the number of the adsorbed chain ends of the long chains and phenol molecules will decrease, as well as the thickness of the adsorbed layer. As a result, the (negative) slip length will start to increase again.

IV. DISCUSSION AND CONCLUSIONS

Let us first turn to a brief discussion on the possible mechanisms of friction in our system. Recalling that the adsorbed chain ends move along the equipotential lines of the surface potential, we conclude that the role of the adsorbed additives is twofold: apart from screening the interaction of the melt with the wall, they also serve as additional obstacles which block the possible paths for the chain ends of the major component. If we ignore the weak entanglement of the chains in the adsorbed layer as well as the motion of the adsorbed chain ends of the minor component over the surface, the situation reduces to a two-dimensional site percolation problem. Each vertex is designated open or closed at random, with a probability p to be closed which is proportional to the concentration of the chain ends of the minor component. Percolation theory predicts that for the site percolation on a hexagonal lattice the critical point of the percolation probability is $p_c=1/2$.[34] Assuming that the transition happens for the 20:1 system (see the inset of Fig. 4) we obtain $p_c \approx 0.47$. Of course, due to the applied shear we have an oriented or directed percolation: our lattice sites shall be assigned with particular orientations, along which the percolative paths are biased.

On the other hand, gradual solidification of the adsorbed layer results in the increase of the friction coefficient, due to the collective motion of the adsorbed molecules: once the surface layer is solidified, the adsorbed molecules cannot move in the direction perpendicular to the shear direction. However, hopping between the hole and bridge sites always involves a motion perpendicular to the shear direction, or, in other words, the hexagonal symmetry of the lattice forbids the motion of the beads along the shear.

Once the surface layer is in a solid state, the relative velocity of the adsorbed layer does not change anymore. However, the ratio between the adsorbed chain ends of long and short molecules still changes. This affects the thickness of the adsorbed layer as well as its entanglement with the rest of the melt. As a result, the shear force on the wall decreases with the increase of the concentration of the additive. A similar scenario has already been discussed in the framework of the mean-field theory.[12–15]

To summarize, we studied the effective boundary conditions for a polymer blend adsorbed on a structured surface. The slip boundary condition observed for a monodispersed melt changes to the no slip at some concentration of the additive. Further increase of the concentration of the additive at the surface leads to the solidification and locking of the motion of the adsorbed surface layer.

Finally, we would like to comment on the importance of the multiscale modeling methods we employ in our studies. As underlined in the introduction, we consider a particular system, which is of high relevance to different fields of modern technology. Our results, despite the particular system considered, are the direct expression of the interplay between specific (electronic-based) molecule-surface interactions and global statistical and dynamical properties of the system, i.e., the interplay between the different scales is the crucial ingredient of the description. The electronic and molecular resolutions, implicit into the parametrization of the model, allows for a level of analysis which is beyond any other existing coarse-grained models or mean-field approaches. In this sense, this study goes beyond the specificity of the system considered and calls for extensions to other systems and experimental tests. The present approach is a route which allows to detect important, otherwise not accessible, properties and sets a new link between theory, experiments, and technology.

ACKNOWLEDGMENTS

[1] G. K. Batchelor, *An Introduction to Fluid Dynamics* (Cambridge University Press, Cambridge, 1967), Vol. 67.

[2] J. C. Maxwell, Philos. Trans. R. Soc. London **170**, 231 (1879).

[3] P. A. Thompson and M. O. Robbins, Phys. Rev. A **41**, 6830 (1990).

[4] C. Cottin-Bizonne, J. L. Barrat, L. Bocquet, and E. Charlaix, Nat. Mater. **2**, 237 (2003).

[5] J. Klein, Annu. Rev. Mater. Sci. **26**, 581 (1996).

[6] M. Aubouy, O. Guiselin, and E. Raphael, Macromolecules **29**, 7261 (1996).

[7] V. A. Harmandaris, K. C. Daoulas, and V. G. Mavrantzas, Macromolecules **38**, 5796 (2005).

[8] P. A. Thompson, G. S. Grest, and M. O. Robbins, Phys. Rev. Lett. **68**, 3448 (1992).

[9] N. V. Priezjev and S. M. Troian, Phys. Rev. Lett. **92**, 018302 (2004).

[10] X. Zhou, D. Andrienko, L. Delle Site, and K. Kremer, Europhys. Lett. **70**, 264 (2005).

[11] M. Cieplak, E. D. Smith, and M. O. Robbins, Science **265**, 1209 (1994).

[12] F. Brochard and P. G. de Gennes, Langmuir **8**, 3033 (1992).

[13] A. Ajdari, F. Brochard-Wyart, P. G. de Gennes, L. Leibler, J. L. Viovy, and M. Rubinstein, Physica A **204**, 17 (1994).

[14] K. A. Smith, M. Vladkov, and J.-L. Barrat, Macromolecules **38**, 571 (2005).

[15] F. Brochard-Wyart, P. G. de Gennes, H. Hervert, and C. Redon, Langmuir **10**, 1566 (1994).

[16] K. Cheah and W. D. Cook, Polym. Eng. Sci. **43**, 1727 (2003).

[17] D. Andrienko, S. Leon, L. Delle Site, and K. Kremer, Macromolecules **38**, 5810 (2005).

[18] S. Namhata, M. J. Guest, and L. M. Aerts, J. Appl. Polym. Sci. **71**, 311 (1999).

[19] J. L. DeRudder, *Handbook of Polycarbonate Science and Technology* (Marcel Dekker, New York, 2000).

[20] L. Morbitzer and U. Grigo, Angew. Makromol. Chem. **162**, 87 (1988).

[21] S. F. Tsai, I. K. Lan, and C. L. Chen, Comput. Theor. Polym. Sci. **8**, 283 (1998).

[22] W. Tschop, K. Kremer, J. Batoulis, T. Burger, and O. Hahn, Acta Polym. **49**, 61 (1998).

[23] W. Tschop, K. Kremer, O. Hahn, J. Batoulis, and T. Burger, Acta Polym. **49**, 75 (1998).

[24] L. Delle Site, C. F. Abrams, A. Alavi, and K. Kremer, Phys. Rev. Lett. **89**, 156103 (2002).

[25] L. Delle Site, S. Leon, and K. Kremer, J. Am. Chem. Soc. **126**, 2944 (2004).

[26] C. F. Abrams and K. Kremer, Macromolecules **36**, 260 (2003).

[27] C. F. Abrams, L. Delle Site, and K. Kremer, Phys. Rev. E **67**, 021807 (2003).

[28] L. Delle Site, A. Alavi, and C. F. Abrams, Phys. Rev. B **67**, 193406 (2003).

[29] S. Leon, L. Delle Site, and K. Kremer, Macromolecules (submitted).

[30] The difference is due to the more specific, angular-dependent, potential used to describe the end-wall attractive interaction in Ref. 17, which can be considered as a refinement of a simpler surface potential used in the current study. This affects the conformations of the adsorbed molecules at the surface but is not critical for the conclusions of the current study: as we will see, the flow boundary conditions are basically specified by the surface concentrations of the adsorbed chain ends of the major and minor components, and are not very sensitive to the conformations of the adsorbed chains.

[31] Note that this is not the case for the pure ($N=20$) system and the 20:5 mixture: the latter has slightly thicker adsorbed layer, which can also be seen from the center-of-mass profiles and the velocity profiles. This effect is most probably due to the stiffness of the relatively short chains of 5 repeat units, which adsorb and force the long chains to stretch away from the wall.

[32] L. Léger, E. Raphaël, and H. Hervet, Adv. Polym. Sci. **138**, 185 (1999).

[33] K. J. Strandberg, *Bond Orientational Order in Condensed Matter Systems* (Springer, Berlin, 1992).

[34] M. F. Sykes and J. W. Essam, Phys. Rev. Lett. **10**, 1 (1963).